

# A 60 GHz Phase Shifter Integrated With LNA and PA in 65 nm CMOS for Phased Array Systems

Yikun Yu, Peter G. M. Baltus, *Member, IEEE*, Anton de Graauw, Edwin van der Heijden, Cicero S. Vaucher, *Senior Member, IEEE*, and Arthur H. M. van Roermund, *Senior Member, IEEE*

**Abstract**—This paper presents the design of a 60 GHz phase shifter integrated with a low-noise amplifier (LNA) and power amplifier (PA) in a 65 nm CMOS technology for phased array systems. The 4-bit digitally controlled RF phase shifter is based on programmable weighted combinations of I/Q paths using digitally controlled variable gain amplifiers (VGAs). With the combination of an LNA, a phase shifter and part of a combiner, each receiver path achieves 7.2 dB noise figure, a  $360^\circ$  phase shift range in steps of approximately  $22.5^\circ$ , an average insertion gain of 12 dB at 61 GHz, a 3 dB-bandwidth of 5.5 GHz and dissipates 78 mW. Consisting of a phase shifter and a PA, one transmitter path achieves a maximum output power of higher than +8.3 dBm, a  $360^\circ$  phase shift range in  $22.5^\circ$  steps, an average insertion gain of 7.7 dB at 62 GHz, a 3 dB-bandwidth of 6.5 GHz and dissipates 168 mW.

**Index Terms**—Active phase shifter, digitally controlled, I/Q signals, low-noise amplifier (LNA), mm-wave, power amplifier (PA), receiver, RF beamforming, RF phase shifting, transmitter, variable gain amplifier (VGA), 60 GHz, 65 nm CMOS,  $90^\circ$  transmission line.

## I. INTRODUCTION

THE 7 GHz unlicensed band around 60 GHz offers exciting opportunities for applications such as high-speed short-range wireless personal area network (WPAN) and real time video streaming at rates of several Gb/s [1]–[3]. Continuous scaling of the CMOS technology results in significant performance improvement, and enables 60 GHz front-ends to be implemented at low cost [4]–[7].

A major issue in designing such a high data rate 60 GHz radio is the limited link budget over indoor distances, especially for the non-line-of-sight (NLOS) situations, due to the high path loss during radio propagation, high noise figure of the receiver and low output power of the transmitter [8], [9]. Due to the relative small size of 60 GHz antennas, the phased array technique is an attractive solution to compensate the path loss

and alleviate the requirements of the RF transceiver front-ends. In addition to providing electronic controlled beam forming, phased arrays offer larger effective isotropic radiated power (EIRP) in the transmitter and higher signal-to-noise ratio (SNR) in the receiver [10]–[15]. This leads to higher system capacity and larger range which is highly beneficial to a 60 GHz wireless system.

Phase shifters are essential components in a phased array for adjusting the phase of each antenna path and steering the beam [16], [17]. Placing the phase shifters in the LO path [18]–[20] or IF path [21]–[24] requires separate frequency converters for each of the antennas, while each frequency converter consists of separate mixers, LO buffers and LO distribution. By placing the phase shifters in the RF path of a receiver/transmitter, the signals from/to each of the antennas are combined/split at RF [Fig. 1(a) and (b), respectively], which shares the frequency converter among the multiple antennas and results in simple system architecture [25]–[28]. An RF phase shifter may require a higher dynamic range as compared to an LO phase shifter. On the other hand, an RF phase shifting approach keeps the floor plan of the LO circuitry simple, i.e., there is only a single mixer (or two in an I/Q scheme) to be driven by the LO signal. This also means that the core circuitry of the receiver and transmitter (up to the mixer) can be reused for different array configurations, without the need to add additional mixers to the circuitry when, for example, increasing the number of antennas. At the end, the number of physical circuit elements is smaller in an RF phase shifting scheme than in an LO phase shifting scheme, leading to a smaller chip area. Another aspect of RF phase shifting is that in the receiver, because of the spatial filtering of interferers at RF, the dynamic range and therefore the power dissipation of the mixers and subsequent stages can be reduced.

The main challenge associated with RF phase shifting is the implementation of low-loss high-resolution RF phase shifters at 60 GHz. This work proposes a 4-bit digitally controlled RF phase shifter that is based on programmable weighted combinations of I/Q paths with digitally controlled variable gain amplifiers (VGAs) [29]. Compared to the passive designs [30]–[34], this phase shifter achieves high gain, small area, large phase shift range ( $360^\circ$ ) and high phase shift resolution ( $22.5^\circ$ ). Instead of using an all-pass polyphase filter [35], [36] or quadrature coupler [34], the I/Q signals are generated using a  $90^\circ$  transmission line that enables low loss and sufficient I/Q accuracy. The gain settings of the VGAs are achieved through digitally controlled current steering by turning on or off a certain number of unit transistors in parallel. The fully digitally controlled phase shifter allows for a simple control and better immunity to the

Manuscript received January 30, 2010; revised March 30, 2010; accepted April 16, 2010. Date of current version August 25, 2010. This paper was approved by Associate Editor Behzad Razavi. This work is supported by the SenTenNovem in The Netherlands.

Y. Yu was with the Department of Electrical Engineering, Eindhoven University of Technology, 5600 MB Eindhoven, The Netherlands. He is now with IMEC, 5605 KN Eindhoven, The Netherlands (e-mail: yikun.yu@imec-nl.nl).

P. G. M. Baltus and A. H. M. van Roermund are with the Department of Electrical Engineering, Eindhoven University of Technology, 5600 MB Eindhoven, The Netherlands.

A. de Graauw, E. van der Heijden, and C. S. Vaucher are with NXP Semiconductors, Research, 5656 AE Eindhoven, The Netherlands.

Color versions of one or more of the figures in this paper are available online at <http://ieeexplore.ieee.org>.

Digital Object Identifier 10.1109/JSSC.2010.2051861

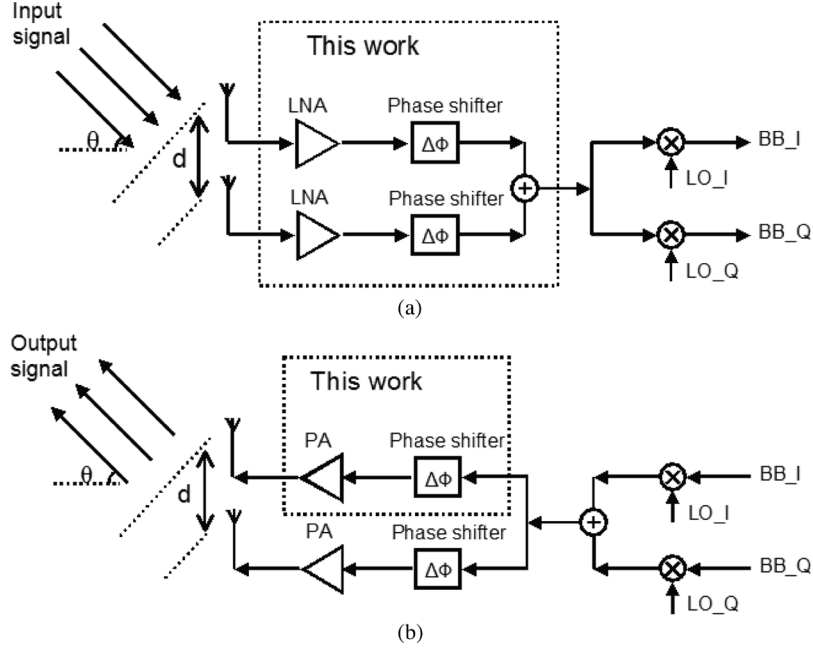


Fig. 1. Block diagram of a 60 GHz phased array (a) receiver and (b) transmitter front-end using RF-path phase shifting.

noise in the control lines. With the use of the proposed 4-bit RF phase shifter, this work designs a 60 GHz two-path receiver in which each path consists of a low-noise amplifier (LNA), a phase shifter and part of a combiner [Fig. 1(a)], and a 60 GHz transmitter path that consists of a power amplifier (PA) and a phase shifter [Fig. 1(b)], both in a 65 nm CMOS technology.

This paper is organized as follows. In Section II, the principle of the proposed RF phase shifter is presented first, followed by the circuit design of the RF phase shifter as well as LNA and PA for 60 GHz phased array systems. The measurement results of the receiver path and the transmitter path are presented and discussed in Section III.

## II. CIRCUIT DESIGN

### A. Principle of the Phase Shifter

In this work, the RF phase shifter has a phase resolution of  $22.5^\circ$  (4-bit resolution) and a phase control range of  $360^\circ$ . The propagation time delay in a phased array system is approximated to a constant phase shift over the signal bandwidth, which may lead to distortion in a system that uses a broadband high order modulation scheme or uses an instantaneously wide bandwidth [37], [38]. System simulation shows that the use of a 4-bit constant phase shifter meets the requirements including error vector magnitude (EVM) and array patterns of a 60 GHz 8-path phased array transceiver, which employs shaped QPSK modulation ( $\beta = 0.5$ ) and has bit rates of 10 Gb/s [9]. The phase shifter has low insertion loss (or even gain), low variation in loss, in this way it is not required to implement an LNA or PA with very high gain, programmable gain settings, and large power dissipation in order to compensate the loss and loss variations. Furthermore, the phase shifter requires sufficient linearity. This is because in the receiver path, the LNA and phase shifter

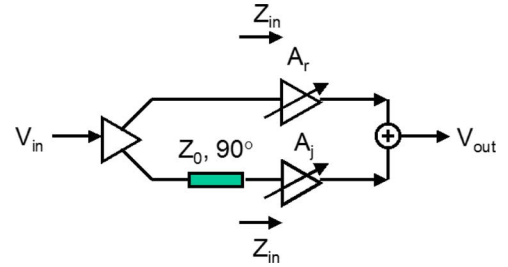


Fig. 2. Block diagram of a phase shifter.

may need to process the desired signals along with strong interferers, whereas beamforming and possible “nulling” of jammer are achieved after signal combining. In the transmitter path the phase shifter should not limit the linearity and output power of the transmitter.

Fig. 2 shows the block diagram of the proposed phase shifter. The input signal ( $V_{in}$ ) is fed through two paths with or without a  $90^\circ$  phase shift, respectively, which generates I/Q signals. These I/Q signals are weighted by separate VGAs ( $A_r$ ,  $A_j$ ) and combined at the output ( $V_{out}$ ). If the input impedance of each VGA ( $Z_{in}$ ) is equal to the characteristic impedance ( $Z_0$ ) of the transmission line, and if there are no gain and phase errors in the I/Q signals, the output signal of the phase shifter can be expressed as

$$V_{out} = (A_r + jA_j)V_{in}. \quad (1)$$

The phase shift achieved is given by

$$\phi = \arctan(A_j/A_r). \quad (2)$$

The gain of the phase shifter can be expressed as

$$A = \sqrt{A_r^2 + A_j^2}. \quad (3)$$

Here  $A_r$  and  $A_j$  are the gains of the two VGAs in the I/Q paths, respectively, which are given by

$$A_r = A_0 \cos(\phi) \quad (4)$$

$$A_j = A_0 \sin(\phi) \quad (5)$$

in which  $\phi$  is the desired phase shift and  $A_0$  is a constant representing the gain of the phase shifter. In this way, the phase shifter achieves a phase shift of  $\phi$  with a constant gain of  $A_0$ .

However, there are often gain errors and phase errors in the weighted I/Q signals before signal combination. This is because, first, the 90° transmission line itself has gain and phase errors. Second, there can be impedance mismatch (and therefore reflection) between the input impedance of each VGA ( $Z_{in}$ ) and the transmission line ( $Z_0$ ). In the 60 GHz broadband system, this impedance mismatch is often more severe due to the variation of impedance ( $Z_{in}$  and  $Z_0$ ) within the band of interest. Third, gain and phase errors can also be contributed by the weighting of the two VGAs. If we model the overall gain errors and phase errors in the weighted I/Q signals as  $\epsilon$  and  $\theta$ , respectively, the output signal ( $V_{out}$ ) of the phase shifter can be expressed as

$$\begin{aligned} V_{out} &= [A_r + A_j(1 - \epsilon)e^{j(\frac{\pi}{2} - \theta)}] V_{in} \\ &\approx [(A_r + \theta A_j) + j A_j(1 - \epsilon)] V_{in} \\ &= [\cos(\phi) + \theta \sin(\phi) + j \sin(\phi)(1 - \epsilon)] A_0 V_{in}. \end{aligned} \quad (6)$$

The phase shift achieved due to the gain and phase errors in the weighted I/Q signals is given by

$$\phi' = \arctan \frac{\sin(\phi)(1 - \epsilon)}{\cos(\phi) + \theta \sin(\phi)}. \quad (7)$$

As compared to the ideal phase shift in (2), the phase error of the phase shifter due to the gain and phase errors in the weighted I/Q signals can be written as

$$\begin{aligned} \Delta\phi &= \phi' - \phi \\ &= \arctan \left[ \frac{-\frac{\theta}{2} - \frac{\epsilon}{2} \sin(2\phi) + \frac{\theta}{2} \cos(2\phi)}{1 - \frac{\epsilon}{2} + \frac{\theta}{2} \sin(2\phi) + \frac{\epsilon}{2} \cos(2\phi)} \right] \\ &\approx -\frac{\theta}{2} - \frac{\epsilon}{2} \sin(2\phi) + \frac{\theta}{2} \cos(2\phi). \end{aligned} \quad (8)$$

The RMS phase errors (in radians) of the phase shifter [26], as compared to an ideal phase shifter, can be expressed as

$$\begin{aligned} \Delta\phi_{RMS} &= \sqrt{\frac{1}{2\pi} \int_0^{2\pi} (\phi' - \phi)^2 d\phi} \\ &\approx \sqrt{\frac{3}{8}\theta^2 + \frac{1}{8}\epsilon^2}. \end{aligned} \quad (9)$$

The gain of the phase shifter with the gain and phase errors in the weighted I/Q signals is given by

$$\begin{aligned} A' &= A_0 \sqrt{(\cos(\phi) + \theta \sin(\phi))^2 + \sin^2(\phi)(1 - \epsilon)^2} \\ &\approx A_0 \sqrt{1 - \epsilon + \theta \sin(2\phi) + \epsilon \cos(2\phi)}. \end{aligned} \quad (10)$$

As compared to an ideal phase shifter, the RMS gain errors (in dBs) [26] of the phase shifter can be expressed as

$$\begin{aligned} \Delta A_{RMS,dB} &= \sqrt{\frac{1}{2\pi} \int_0^{2\pi} (A'_{dB} - A_{0,dB})^2 d\phi} \\ &\approx 8.7 \sqrt{\frac{1}{8}\theta^2 + \frac{3}{8}\epsilon^2}. \end{aligned} \quad (11)$$

From (9) and (11), for example, in order to design a 4-bit phase shifter with RMS gain and phase errors of less than 1.7 dB and 11.25°, respectively, we have  $\epsilon \leq 0.28$  and  $\theta \leq 0.28$ . In other words, in comparison to an ideal phase shifter with perfect I/Q signal generation and weighting, the gain and phase errors in the weighted I/Q signals before signal combination are less than 2.8 dB and 16°, respectively. It is worth pointing out that a 90° transmission line contributes less than 9° phase error within 20% bandwidth at 60 GHz. Therefore, it is used, instead of using a true time delay scheme, to generate the broadband I/Q signals.

In order to generate 4-bit phase shifts, the gain ratio of the two VGAs in the I/Q paths ( $A_j/A_r$ ) are programmed in certain discrete settings such as 0/3, 1/3, 2/2, 3/1, or 3/0, in this way the phase shift can vary between 0° to 90° in a step of approximately 22.5°. By changing the polarity of  $A_r$  and  $A_j$  independently, a phase control range of 360° can be achieved, which can be done by swapping the positive and negative paths in the differential circuits of the two VGAs. Note that the gain ratio settings of  $A_j/A_r$  are set to 1/3 or 3/1 in order to achieve phase shift of 22.5 or 67.5°, since these ratio settings are simpler to be implemented as compared to the exact gain ratios of 1/2.4 or 2.4/1 for these phase shifts. The resulted gain and phase errors in the phase shifter due to these simplified gain ratio settings are well acceptable. As compared to an ideal 4-bit phase shifter, this phase shifter achieves a peak-to-peak gain variation of less than ±0.5 dB and a peak-to-peak phase error of less than 4° across different phase settings in simulation, when used in combination with ideal I/Q signals. The phase shifter can be extended to achieve higher phase resolution, for example, 5 bits, by programming  $A_j/A_r$  in more discrete settings.

As shown in Fig. 3(a), the 90° transmission line is implemented using a differential coplanar transmission line in a ground-signal-ground-signal-ground (GSGSG) configuration. The signal lines are using the top metal layer (metal-7). The ground lines are using the top metal layer (metal-7) that are connected to the bottom metal layer (metal-1) through vias, and form a solid ground plane using the bottom metal layer (metal-1) underneath the signal lines. The width and spacing of the signal lines and ground lines are all 4 μm at the top metal layer (metal-7). This transmission line has a measured differential impedance  $Z_{diff} = 100 \Omega$ , a relative dielectric

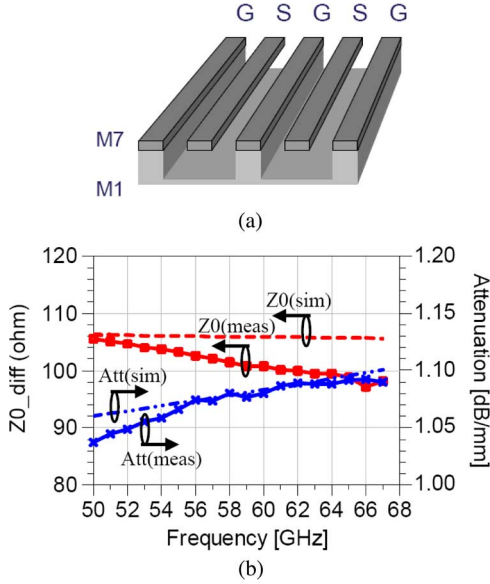


Fig. 3. (a) A differential coplanar (GSGSG) transmission line, in which the signal lines use the top metal layer (metal-7), and there is a solid ground plane using the bottom metal layer (metal-1) underneath the signal lines, and (b) its measurement results.

constant ( $\epsilon_r$ ) of 3.8, an attenuation of 1.08 dB/mm at 60 GHz which match the simulated results [Fig. 3(b)]. The difference between simulated and measured  $Z_{diff}$  is probably due to the accuracy of de-embedding, since there are open and short stubs used as test structures [31], whereas load and through structures are not available. The  $90^\circ$  transmission line has a width of  $36 \mu\text{m}$ , a total length of  $650 \mu\text{m}$ , and an insertion loss of 0.7 dB at 60 GHz.

### B. Design of the Phase Shifter for the Receiver

Fig. 4 shows the schematic of the phase shifter for the receiver. The input transconductance stage,  $90^\circ$  line, and two digitally controlled VGAs are merged in a common-source cascode configuration for low power, high gain, and stability considerations. The input transconductance stage ( $M_1$ – $M_4$ ) converts the signal ( $V_{in+}$  and  $V_{in-}$ ) into separate currents. I/Q signals are generated by feeding these currents through two paths with and without a  $90^\circ$  transmission line, respectively. Two digitally controlled VGAs weigh these I/Q signals separately and generate the required phase at the combined output ( $V_{out+}$  and  $V_{out-}$ ). The shunt transmission line ( $L_p$ ) cancels the impedance contributed by the input capacitance of the VGA at 60 GHz. The real part of the input impedance of each VGA ( $Z_{in}$ ) is chosen to be equal to the characteristic impedance of the  $90^\circ$  transmission line ( $Z_0$ ).

The VGAs in the phase shifter are implemented using a common-gate configuration as shown in Fig. 5. The gain is programmed by switching on or off a certain number of unit transistors, which are connected to  $V_{out+}$ ,  $V_{out-}$ , or  $V_{dd}$ , respectively. The connections of these transistors are based on the digital control at their gates. In this way, the desired portion of the input currents of each VGA is diverted to the output, while the remaining portion is fed into the supply. For example, if 1/4 of the input current of the I-path VGA and 3/4 of the input

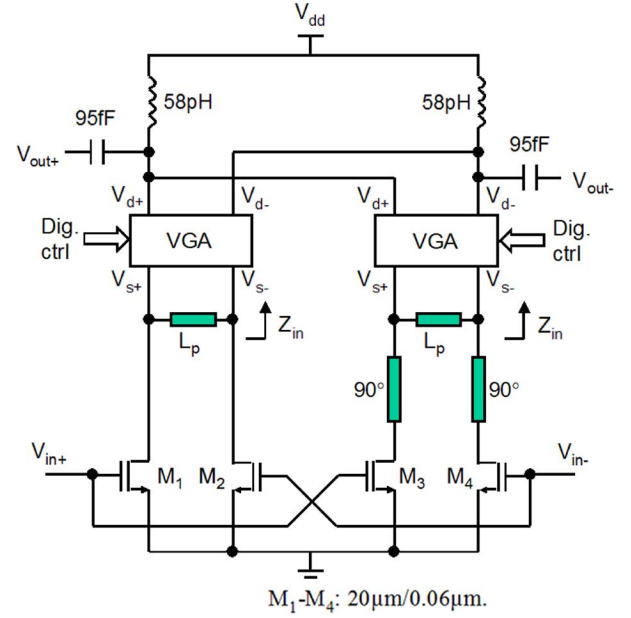


Fig. 4. Schematic of a 60 GHz 4-bit phase shifter in the receiver.

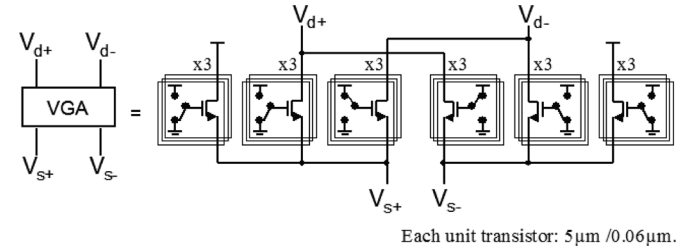


Fig. 5. Schematic of a VGA in the phase shifter of the receiver.

current of the Q-path VGA are diverted to the output, the gain ratio of the two VGAs ( $A_j/A_r$ ) is 3/1, therefore the phase shift achieved is approximately  $67.5^\circ$ . By programming  $A_j/A_r$  to 0/3, 1/3, 2/2, 3/1, or 3/0 as well as changing the polarity of  $A_r$  and  $A_j$ , the phase shifter achieves a phase control range of  $360^\circ$  in steps of approximately  $22.5^\circ$ . This current steering approach provides a phase shift that is in the first order insensitive to the variations in technology, supply voltage, and temperature (PVT), since the phase shift is set by the gain ratio and therefore the number of unit transistors that connects to the output of the two VGAs. Moreover, by using the dummy transistors that connect to  $V_{dd}$ , the total number of unit transistors switched on is constant. In this way, the variations of the VGA input impedance are minimized, which provides the broadband load impedance required at the output of the  $90^\circ$  transmission line.

In simulation, the phase shifter in the receiver (Fig. 4) has an average insertion gain of 0 dB, an output referred 1dB-compression point ( $P_{1dB}$ ) of  $-9$  dBm at 60 GHz and consumes 19.5 mW.

### C. Design of the LNA and Combiner for the Receiver

Thanks to the phase shifter with low loss, the requirements of the LNA are low noise figure, reasonable gain, and low power consumption. The two-stage differential LNA is shown in Fig. 6. The common-source cascode configuration offers low noise,

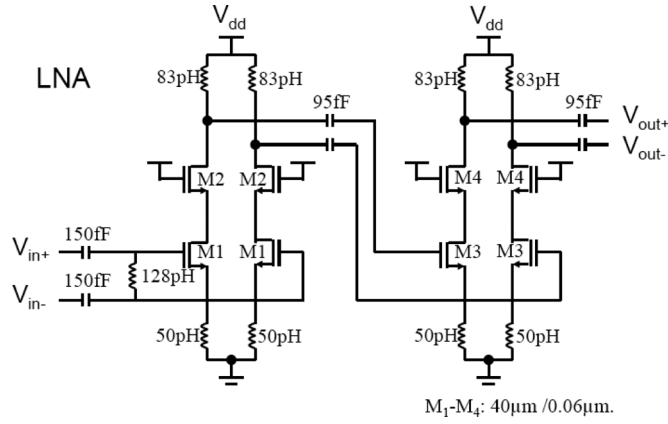


Fig. 6. Schematic of a 60 GHz LNA.

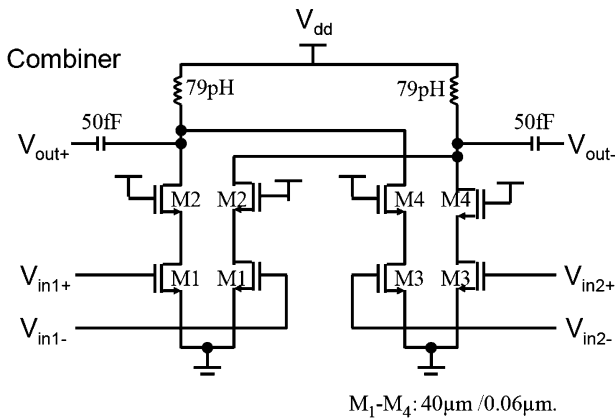


Fig. 7. Schematic of a 60 GHz combiner.

high gain and stability. The input of the receiver is matched to  $100\ \Omega$  differential antennas [39]. There is inductive degeneration at the source of the input transistors to provide broadband power and noise matching. Measured results shows that a stand-alone LNA has a measured minimum noise figure of 5.5 dB and a power gain of 8.4 dB at 61 GHz [29]. The 3 dB bandwidth is 10.4 GHz. The LNA consumes 39 mW.

The combiner that follows the phase shifters is shown in Fig. 7. The RF signals from the two antenna paths are fed into two common-source cascode amplifiers. Subsequently, the signals are combined at the outputs of these amplifiers. The output of the combiner is matched to  $100\ \Omega$  differentially for measurement purpose. The common-source cascode configuration provides isolation between the two paths. It achieves a simulated insertion gain of 4 dB (from  $V_{in1}$  or  $V_{in2}$  to  $V_{out}$ ) at 60 GHz and consumes 19.5 mW. This implementation of power combiner has a higher gain than the use of a passive power combiner (such as a Wilkinson power combiner [26]). It is worth pointing out that by connecting more amplifiers in parallel, this combining method can be scaled to more paths. However, for a large number of paths, the output impedance of the combiner may be reduced significantly. Therefore, it becomes difficult to drive the load impedance of the combiner (i.e., the input impedance of the mixer). The loading problem can be solved by using multiple combiner stages in a tree

structure to combine a large number of paths while maintaining sufficient output impedance [24].

The spiral inductors in this work use the top two metal layers (metal-7 and metal-6) as signal paths and the bottom metal layer (metal-1) as a patterned ground shield, and are implemented using single-turn differential inductors with center tap. Simulations using the LSIM 3.1 tool [40] shows that the quality factors of the inductors are higher than 20 at 60 GHz. The capacitors are implemented using the intermediate metal layers stacking from metal-2 to metal-5, with minimum-spacing interdigitated fingers fringe capacitor configuration. In the simulation these capacitors have quality factors of around 10 at 60 GHz.

To achieve optimal noise figure and power gain, the finger width of the MOS transistors is chosen to be  $1\ \mu\text{m}$  and the DC current density is approximately 0.15 mA per  $\mu\text{m}$ -gate-width. Wideband matching networks are adopted in order to provide broadband performance with low sensitivity to modeling inaccuracies and process variations. Extensive parasitic extractions have been performed on the layouts and taken into account during the circuit simulation. Long on-chip interconnect lines are implemented as transmission lines. The supply voltage in the receiver path is 1.5 V in order to provide voltage headroom in the cascode topologies. Since the gates of the cascode transistors are all connected to 1.5 V, within the 1 dB compression point the voltage swings at the inductive loads are less than the threshold voltage ( $V_{TH}$ ) of the transistors. The cascode structures help to reduce the voltage stress on each transistor well below the specified breakdown voltage.

#### D. Design of the Phase Shifter for the Transmitter

The phase shifter in the transmitter has high linearity requirement, so that it is the output stage of the power amplifier rather than the phase shifter that saturates first, otherwise the overall efficiency of the transmitter is decreased.

The schematic of the phase shifter in the transmitter is depicted in Fig. 8. Its operating principle is similar to that in the receiver (Fig. 4). The RF signal ( $V_{in+}$  and  $V_{in-}$ ) is converted into separate currents by a transconductance stage (M1–M4). I and Q signals are generated by feeding these currents through two paths with or without a  $90^\circ$  line, and weighted by the digitally controlled VGAs separately. The required phase is generated at the combined output ( $V_{out+}$  and  $V_{out-}$ ). As compared to the implementation in the receiver that merges the transconductance stage and the VGAs in a common-source cascode configuration, the phase shifter in the transmitter cascades the transconductance stage and the VGAs in two separate stages, in order to achieve a larger voltage swing and higher output  $P_{1dB}$ . Furthermore, there is inductive degeneration at the source of the input transconductance stage in order to provide input impedance matching ( $100\ \Omega$  differentially) for measurement purposes. The VGAs that are used in the phase shifter are shown in Fig. 9. They are similar to those in the receiver (Fig. 5) that program the gain by switching on or off a certain number of unit transistors. The only difference between the VGAs in the receiver and in the transmitter lies in the DC bias voltage at the gate of the transistors in order to work properly: in Fig. 9 the gate bias of each transistor is either  $V_b$

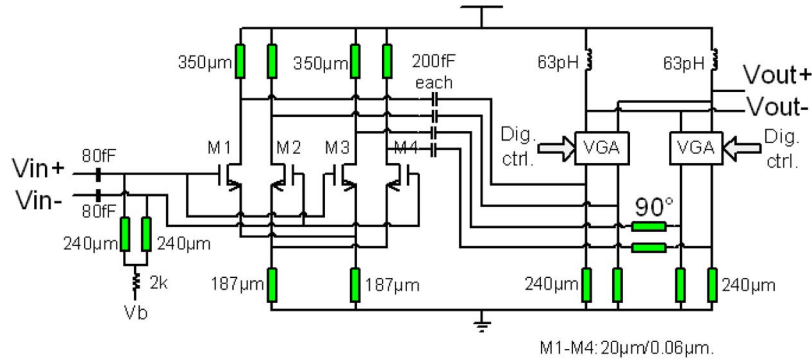


Fig. 8. Schematic of a 60 GHz 4-bit phase shifter in the transmitter.

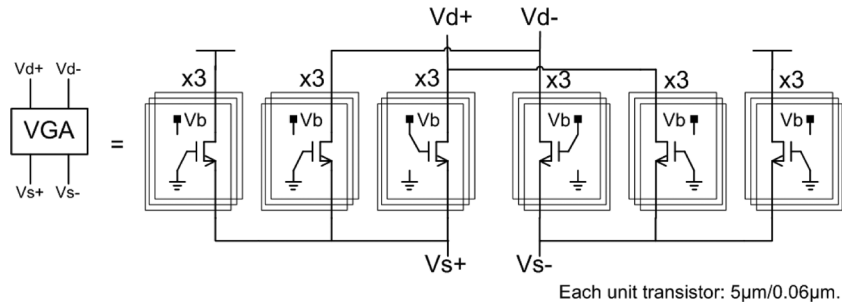


Fig. 9. Schematic of a VGA in the phase shifter of the transmitter.

(DC bias voltage, which is 0.7 V) or 0, instead of being either  $V_{dd}$  or 0 in Fig. 5.

In simulation the phase shifter in the transmitter (Fig. 8) achieves an average insertion gain of  $-6$  dB, an output  $P_{1dB}$  of  $-2$  dBm at 60 GHz and consumes 25 mA from a 1.2 V supply. It features a higher output  $P_{1dB}$  than that in the receiver. In this way the power amplifier instead of the phase shifter limits the linearity of the transmitter. The insertion gain of the phase shifter is lower than that in the receiver, mainly because of its inductive source degeneration that achieves input matching for measurement purposes.

#### E. Design of the PA for the Transmitter

Thanks to the phased array system that can increase the effective isotropic radiated power (EIRP) of a transmitter by spatial power combining, the output power of an individual power amplifier is less critical.

A power amplifier is often designed using a common-source or common-source cascode configuration. In a common-source configuration, the Miller capacitance ( $C_{gd}$ ) reduces the gain, reverse isolation and stability. Therefore, the common-source topology is conditionally stable, which is prone to instability because of the limited accuracy in the transistor model and in the matching network at this high frequency. A common-source cascode structure improves the devices stability but has the disadvantage of reduced voltage headroom and drain efficiency. In this work, the Miller capacitance of a common-source configuration is compensated using neutralization capacitors cross-connected between the drains and gates of the pseudo-differential transistors. As compared to a common-source cascode

configuration, this common-source configuration provides a large output swing. The neutralization capacitors in this work use MOS transistors with the gate as one capacitor terminal and the drain and source connected together as the other capacitor terminal. By properly sizing the MOS transistors, these MOS-transistor-based neutralization capacitors match the Miller capacitors of the common-source amplifiers and are less sensitive to the variations in PVT. In this way, the Miller effect is compensated and stability is ensured. This is an advantage compared to neutralization by the use of fixed parallel-plate metal capacitors as in [41].

Fig. 10 shows the three-stage power amplifier in this work. The output of the power amplifier connects to  $100\ \Omega$  differential antennas [39], and the output matching network of the power amplifier is designed through large-signal load-pull simulation to achieve large output power and high power efficiency. The inductors at the drains and gates of the transistors connect to the supply voltage ( $V_{dd}$ ) and bias voltage  $V_b$ , respectively. These inductors, together with the series fringe capacitors and the shunt transmission line ( $300\ \mu\text{m}$  at the output), form the input, output, and inter-stage matching networks. The total gate width of the transistors in each stage of the power amplifier doubles progressively, which ensures that the output stage saturates first if each stage has at least 3 dB power gain. To achieve an optimal power gain performance, the gate finger width of the MOS transistors is chosen to be  $1\ \mu\text{m}$  with gate contacts at both sides and the DC current density is approximately 0.2 mA per  $\mu\text{m}$ -gate-width. In simulation the power amplifier achieves an insertion gain of 15 dB and a maximum output power ( $P_{max}$ ) of +11 dBm at 60 GHz.



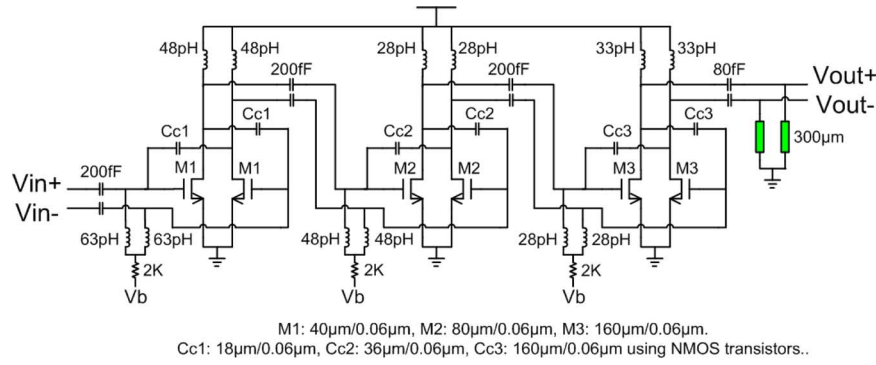


Fig. 10. Schematic of a 60 GHz three-stage power amplifier.

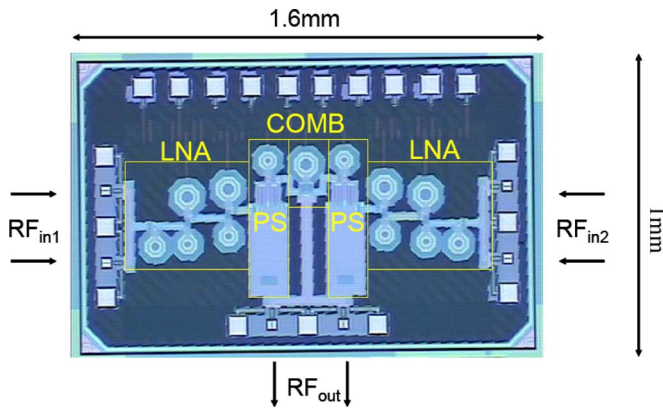


Fig. 11. Chip photo of a two-path 60 GHz receiver in which each path consists of an LNA, a phase shifter, and part of a combiner.

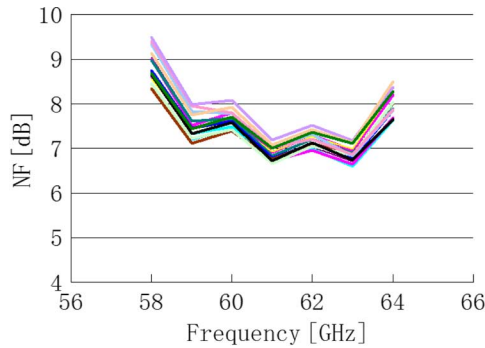


Fig. 12. Measured noise figure of one receiver path for 16 phase settings.

### III. MEASURED RESULTS AND DISCUSSIONS

#### A. Measurements of the Receiver Path

As shown in Fig. 1(a), a two-path 60 GHz receiver is implemented in a 65 nm CMOS technology, in which each path consists of an LNA, a 4-bit RF phase shifter, and part of a combiner (a common-source cascode amplifier). Each phase shifter is controlled independently using digital inputs that are loaded to the phase shifter by a serial peripheral interface (SPI). Fig. 11 shows the die photo. The die area is 1.6 mm<sup>2</sup> and the active circuit occupies 0.9 mm<sup>2</sup>. The layout is symmetrical between the two receiver paths.

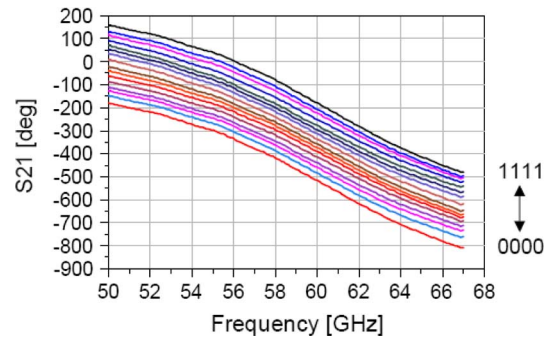


Fig. 13. Measured insertion phase of one receiver path for 16 phase settings.

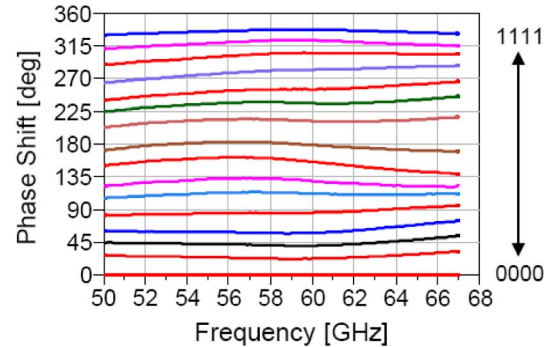


Fig. 14. Measured relative phase shift of one receiver path for 16 phase settings.

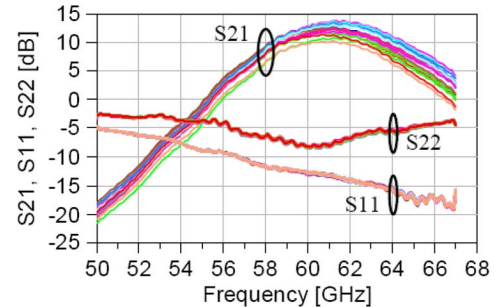


Fig. 15. Measured insertion gain, input and output matching of one receiver path for 16 phase settings.

Each receiver path consumes 52 mA from a 1.5 V supply, in which the LNA, phase shifter, and part of a combiner consumes 26 mA, 13 mA, and 13 mA, respectively.

Fig. 12 shows the measured noise figure of one receiver path for 16 digitally controlled phase settings. The noise figure is

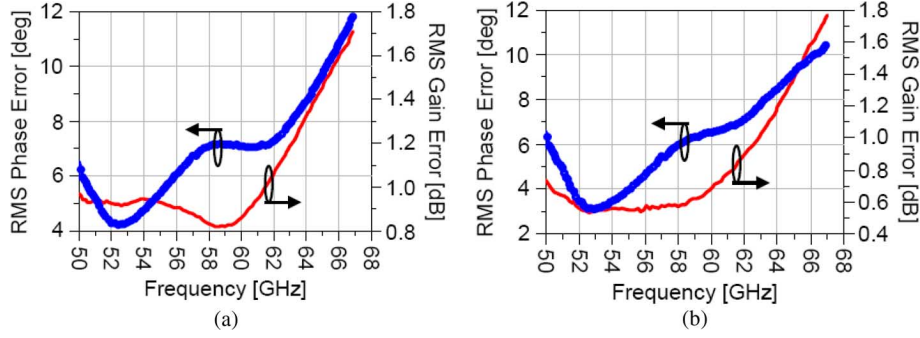


Fig. 16. Measured RMS gain and phase errors: (a) of the 16 phase states and (b) of the I and Q signals in the receiver as compared to an ideal 4-bit phase shifter.

between 6.7 to 7.2 dB across all phase settings at 61 GHz, which is mainly contributed by the LNA with a measured noise figure of 5.5 dB.

The measured insertion phase [ $\text{phase}(S_{21})$ ] of one receiver path for 16 phase settings is depicted in Fig. 13. The phase step is approximately  $22.5^\circ$  (4-bit resolution) and the phase control range is  $360^\circ$  in the 60 GHz band.

Fig. 14 highlights the relative phase shifts of one receiver path for 16 phase settings by setting the phase state 0000 as a reference. This shows that the 4-bit phase shifts achieved are relatively constant over a wide frequency range, which is due to the broadband I/Q signal generation and the frequency insensitive gain ratio of the two VGAs that weigh these I/Q signals.

Fig. 15 presents the measured insertion gain ( $S_{21}$ ), input and output return loss ( $S_{11}$  and  $S_{22}$ ) of one receiver path for 16 phase settings. At the center frequency of 61 GHz, the average insertion gain is 12 dB, and the peak-to-peak gain variation is 3.4 dB across all phase settings. The 3 dB bandwidth is 5.5 GHz. This insertion gain is contributed separately by the LNA that has measured gain of 8.6 dB, the part of the combiner that has a simulated gain of 4 dB, and the phase shifter that has a simulated average gain of 0 dB. The measured  $S_{11}$  and  $S_{22}$  of one receiver path for 16 phase settings are  $-13$  dB and  $-8$  dB, respectively, at 61 GHz, which are determined by the input matching of the LNA and the output matching of the combiner separately and do not change for different phase settings.

Derived from the measured insertion gain and phase shifts, Fig. 16(a) shows the RMS gain and phase errors of the 16 phase states. They are 0.9 dB and  $7^\circ$  at 61 GHz, respectively, as compared to an ideal 4-bit phase shifter with a uniform gain. As highlighted in Fig. 16(b), the RMS gain and phase errors of the I/Q signals, which are measured indirectly using phase state  $0^\circ$ ,  $90^\circ$ ,  $180^\circ$ , and  $270^\circ$ , are 0.8 dB and  $6.8^\circ$ , respectively, at 61 GHz. These frequency dependent gain and phase errors are contributed by the  $90^\circ$  transmission line, the impedance mismatch between the input of each VGA ( $Z_{in}$ ) and the transmission line ( $Z_0$ ), as well as the layout mismatch in the pseudo-differential paths.

Fig. 17 shows the measured nonlinearity of one receiver path. The power gain and output power are plotted as a function of the RF input power at 61 GHz. The measured input referred  $P_{1dB}$  of one receiver path is observed to be  $-16$  dBm at 61 GHz. This  $P_{1dB}$  is limited by the input transconductance stages of

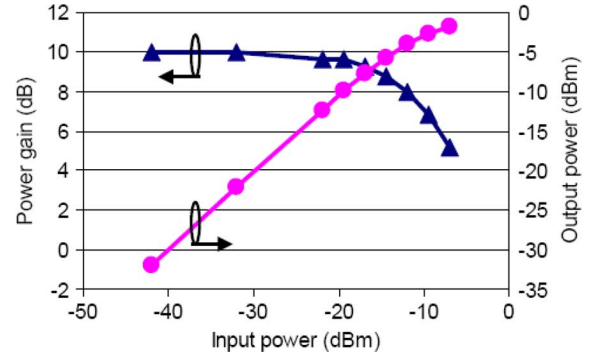


Fig. 17. Measured power gain and output power of one receiver path at 61 GHz versus the RF input power.

the phase shifter and can be improved by, i.e., using source degeneration at the cost of reduced gain and/or increased power consumption.

The measured isolation between the two input ports of the receiver is  $-43$  dB, thanks to the pseudo-differential cascode topologies with differential inductors used in the LNA, phase shifter and combiner.

The mismatches of the two receiver paths are measured through two-port S-parameter measurements in either of the two paths over different phase settings. By comparing the S-parameters of the two paths for the same phase settings, the insertion gain and phase mismatches of the two paths are quantified as RMS gain mismatch and RMS phase mismatch [26]. The measured RMS gain and phase mismatch of the two paths are 0.4 dB and  $2.1^\circ$ , respectively, at 61 GHz. Since the layout of the two receiver paths are symmetrical to each other, these mismatch results are mainly due to the measurement inaccuracies brought by probe placement and cable stability when measuring one of the two paths at a time.

Table I summarizes the measured performance of the receiver path in comparison with reported prior work of mm-wave RF-path phase shifting receivers.

#### B. Measurements of the Transmitter Path

Consisting of a 4-bit digitally controlled RF phase shifter and a power amplifier, a 60 GHz transmitter path is implemented in a 65 nm CMOS technology [Fig. 1(b)]. Expansion of one path to multiple antenna paths can be straightforward, in which the RF



TABLE I  
BENCHMARK OF mm-WAVE RF-PATH PHASE SHIFTING RECEIVERS

Specifications	[26]	[36]	[34]	[25]	This work
Frequency (GHz)	12	77	60	60	61
Phase shifting @	RF	RF	RF	RF	RF
Number of paths	8	1	1	4	2
Key building blocks	LNA + phase shifter + combiner	LNA + phase shifter	phase shifter	LNA + phase shifter + combiner	LNA + phase shifter + combiner
Power Gain of each path (dB)	24.5	$\leq 17$	-2	$\geq 8$	12 (average)
Phase shift step ( $^{\circ}$ )	Digital, 22.5	Analog (+DAC)	Analog (+DAC)	Analog	Digital, 22.5
NF of each path (dB)	4.2	4 (LNA only)	17	$\leq 6.9$	$\leq 7.2$
Input $P_{1dB}$ of each path (dBm)	-33	-	-7	-33.5	-16
Power consumption (mW)	660 (8 paths)	128 (1 path)	32 (1 path)	265 (4 paths)	156 (2 paths)
Technology	0.18 $\mu$ m SiGe Bi-CMOS	0.13 $\mu$ m SiGe Bi-CMOS	0.13 $\mu$ m SiGe Bi-CMOS	0.12 $\mu$ m SiGe Bi-CMOS	65nm CMOS
Chip area (mm <sup>2</sup> )	5.39	0.46	1.48	4.6	1.6

signal from a shared frequency up-converter can be split, phase shifted, amplified and fed into the multiple antennas. Fig. 18 shows the chip photo. The chip area is 1.3 mm  $\times$  1.3 mm and the active area is only 0.8 mm  $\times$  0.4 mm. The transmitter path draws 140 mA from a 1.2 V supply, in which the phase shifter and PA draws 25 mA and 115 mA, respectively.

The measured insertion phase [phase(S21)] of one transmitter path for 16 digitally controlled phase settings is depicted in Fig. 19. It achieves a phase step of approximately 22.5 $^{\circ}$  and a phase control range of 360 $^{\circ}$  in the 60 GHz band.

Fig. 20 shows the measured insertion gain (S21), input and output reflection coefficients (S11 and S22) of one transmitter path for 16 phase settings. It has an average insertion gain of 7.7 dB at 62 GHz and a 3 dB bandwidth of 6.5 GHz, which

match the simulated S21 of phase state 0000. This insertion gain is contributed separately by the phase shifter that has a simulated insertion gain of -6 dB, and the power amplifier that has a simulated gain of 15 dB. The measured S11 and S22 are all better than -8 dB at 62 GHz, which are determined by the input matching of the phase shifter and the output matching of the power amplifier, respectively, and do not change for different phase settings. Besides, the measured reversed isolation (S12) of the transmitter path is -44 dB.

Based on the measured insertion gain and phase shifts, the RMS gain and phase errors of one transmitter path are shown in Fig. 21. They are 1.2 dB and 9.2 $^{\circ}$  at 62 GHz, respectively, as compared to an ideal 4-bit phase shifter with a uniform gain. The phase accuracy meets the 4-bit requirement.

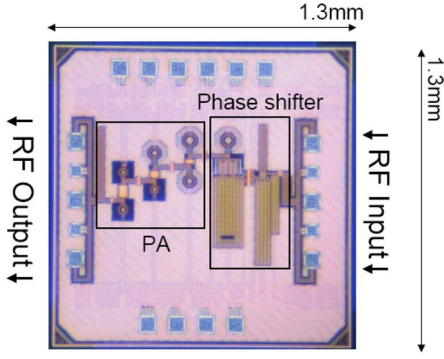


Fig. 18. Chip photo of a 60 GHz transmitter path that combines a phase shifter and a PA.

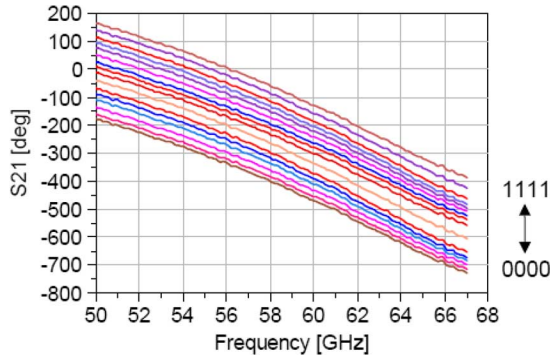


Fig. 19. Measured insertion phase of one transmitter path for 16 phase settings.

Fig. 22 presents the measured nonlinearity of one transmitter path and compares to the simulated result. The measured output  $P_{1dB}$  is +4 dBm at 62 GHz. The measured maximum output power ( $P_{max}$ ) of one transmitter path is observed to be higher than +8.3 dBm (limited by the test equipment) with a corresponding power-added efficiency (PAE) of 2.4%. Considering that the phase shifter has a simulated loss of 6 dB and consumes 30 mW, the power amplifier has a corresponding gain of approximately 10 dB and a PAE of 4.4% when transmitting this output power. The power gain, output power and efficiency of the power amplifier can be further improved using a transformer coupled input, interstage and output matching network [41], [42], as the insertion loss of the matching network can be reduced without the use of lossy passive components including spiral inductors, fringe capacitors, and long interstage interconnects.

Table II summarizes the measured performance of the transmitter path in comparison with previously published works. Although the comparison is not totally fair in the sense that we describe a single channel, it is still useful.

#### IV. CONCLUSION

In this work we have presented a 60 GHz phase shifter integrated with LNA and PA in 65 nm CMOS for phased array systems. The operation of the 4-bit RF phase shifter is based on programmable weighted combinations of I/Q paths using digitally controlled VGAs. The RF phase shifter achieves a 360° phase

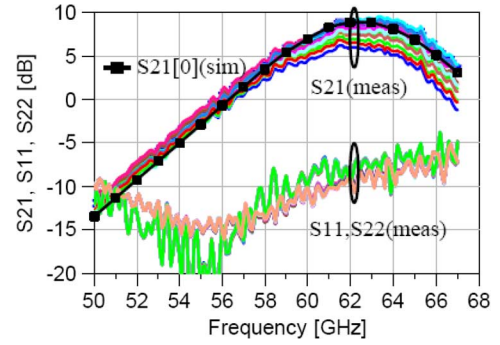


Fig. 20. Measured insertion gain, input and output matching of one transmitter path for 16 phase settings.

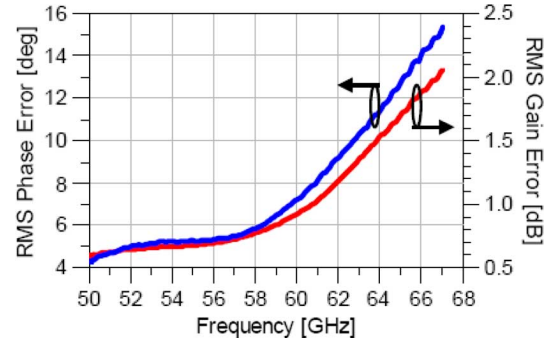


Fig. 21. Measured RMS gain and phase errors of the 16 phase states in the transmitter as compared to an ideal 4-bit phase shifter.

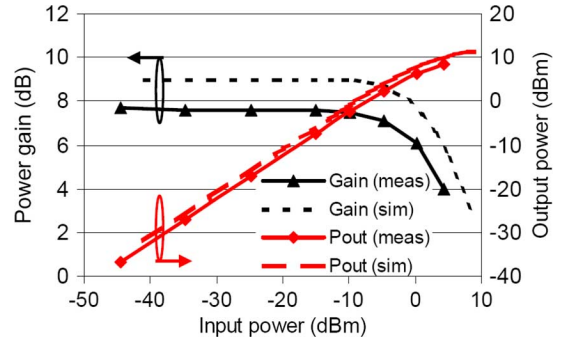


Fig. 22. Measured power gain and output power of one transmitter path at 62 GHz versus the RF input power.

shift range in approximately 22.5° steps for both the 60 GHz receiver and transmitter. Consisting of an LNA, a phase shifter, and part of a combiner, each receiver path achieves 7.2 dB noise figure and an average insertion gain of 12 dB at 61 GHz. With the combination of a phase shifter and a PA, one transmitter path achieves a maximum output power of higher than +8.3 dBm and an average insertion gain of 7.7 dB at 62 GHz. This work has demonstrated that RF phase shifting is an appealing technique for 60 GHz phased arrays: it achieves sufficient phase resolution (4-bit), large phase range (360°), full integration in CMOS, low supply voltage, and low power consumption, consumes small chip area, and possesses further scalability towards larger phased arrays without modification of the existing frequency converter and LO distribution network.

TABLE II  
BENCHMARK OF mm-WAVE PHASED ARRAY TRANSMITTERS

Specifications	[18]	[27]	[28]	[20]	This work
Frequency (GHz)	77	42.5	60	60	62
Phase shifting @	LO	RF	RF	LO	RF
Number of paths	4	16	16	4	1
Key building blocks	PA + mixer + VCO + phase shifter + frequency divider, etc.	PA + phase shifter + signal divider, etc.	PA + phase shifter + mixer + RF power distribution + frequency synthesizer, etc.	PA + mixer + phase shifter + LO tripler, etc.	PA + phase shifter
Power Gain of each path (dB)	40.6 (@base-band)	12.5	35 (max @baseband)	20 (@baseband)	7.7 (average)
Max. output power of each path (dBm)	+12.5	-2.5	+9 ( $P_{out,dB}$ )	+11	$\geq +8.3$
Phase shift step ( $^{\circ}$ )	Analog	Digital, 22.5	Digital, 11.25	Analog	Digital, 22.5
Supply voltage (V)	2.5&1.5	5&3.3	2.6	1	1.2
Power consumption (mW)	1828 (4 paths)	3600 (16 paths)	3800 (16 paths)	590 (4 paths)	168 (1 path)
Technology	0.12 $\mu$ m SiGe Bi-CMOS	0.18 $\mu$ m SiGe Bi-CMOS	0.12 $\mu$ m SiGe Bi-CMOS	65nm CMOS	65nm CMOS
Chip area (mm <sup>2</sup> )	17	8.3	43.9	4.1	1.7

#### ACKNOWLEDGMENT

The authors thank Dr. Raf Roovers, Dennis Jeurissen, Manel Collados, Dr. Mark van der Heijden, Mustafa Acar in the Research Department of NXP Semiconductors, Prof. Lawrence E. Larson at the University of California at San Diego for help in this work, Piet Klessens in the Eindhoven University of Technology for help in the measurement, and SenterNovem for funding the project.

#### REFERENCES

- [1] P. Smulders *et al.*, "Exploiting the 60 GHz band for local wireless multimedia access," *IEEE Commun. Mag.*, vol. 2, no. 1, pp. 140–147, Jan. 2002.
- [2] S. E. Gunnarsson *et al.*, "60 GHz single-chip front-end MMICs and systems for multi-Gb/s wireless communication," *IEEE J. Solid-State Circuits*, vol. 42, no. 5, pp. 1143–1157, May 2007.
- [3] B. Floyd *et al.*, "A 60-GHz CMOS receiver front-end," *IEEE J. Solid-State Circuits*, vol. 40, no. 1, pp. 156–167, Jan. 2005.
- [4] C. H. Doan *et al.*, "Millimeter wave CMOS design," *IEEE J. Solid-State Circuits*, vol. 40, no. 1, pp. 144–155, Jan. 2005.
- [5] B. Razavi, "A 60-GHz CMOS receiver front-end," *IEEE J. Solid-State Circuits*, vol. 41, no. 1, pp. 17–22, Jan. 2006.

- [6] C. Marcu *et al.*, "A 90 nm CMOS low-power 60 GHz transceiver with integrated baseband circuitry," in *IEEE Int. Solid-State Circuits Conf. (ISSCC) Dig. Tech. Papers*, 2009.
- [7] J. Borremans *et al.*, "A digitally controlled compact 57-to-66 GHz front-end in 45 nm digital CMOS," in *IEEE Int. Solid-State Circuits Conf. (ISSCC) Dig. Tech. Papers*, 2009.
- [8] A. M. Niknejad *et al.*, *mm-Wave Silicon Technology: 60 GHz and Beyond*. New York: Springer, 2008.
- [9] P. Baltus *et al.*, "Systems and architectures for very high frequency radio links," in *Analog Circuit Design*. New York: Springer, 2008.
- [10] G. E. Moore, "Cramming more components onto integrated circuits," *Electronics*, vol. 38, no. 8, pp. 114–117, Apr. 1965.
- [11] D. Parker *et al.*, "Phased arrays—Part I: Theory and architectures," *IEEE Trans. Microw. Theory Tech.*, vol. 50, no. 3, pp. 678–687, Mar. 2002.
- [12] D. Parker *et al.*, "Phased-arrays C part II: Implementations, applications, and future trends," *IEEE Trans. Microw. Theory Tech.*, vol. 50, no. 3, pp. 688–698, Mar. 2002.
- [13] X. Guan *et al.*, "A fully integrated 24-GHz eight-element phased-array receiver in silicon," *IEEE J. Solid-State Circuits*, vol. 39, no. 12, pp. 2311–2320, Dec. 2004.
- [14] A. Natarajan *et al.*, "A fully integrated 24-GHz phased-array transmitter in CMOS," *IEEE J. Solid-State Circuits*, vol. 40, no. 12, pp. 2502–2514, Dec. 2005.
- [15] H. Hashemi *et al.*, "A 24-GHz SiGe phased-array receiver—LO phase-shifting approach," *IEEE Trans. Microw. Theory Tech.*, vol. 53, no. 2, pp. 614–625, Feb. 2005.
- [16] A. Afsahi *et al.*, "A low-power single-weight-combiner 802.11abg SoC in 0.13  $\mu\text{m}$  CMOS for embedded applications utilizing an area and power efficient Cartesian phase shifter and mixer circuit," *IEEE J. Solid-State Circuits*, vol. 43, no. 5, pp. 1101–1118, May 2008.
- [17] J. Paramesh *et al.*, "A four-antenna receiver in 90-nm CMOS for beam-forming and spatial diversity," *IEEE J. Solid-State Circuits*, vol. 40, no. 12, pp. 2515–2524, Dec. 2002.
- [18] A. Natarajan *et al.*, "A 77-GHz phased-array transceiver with on-chip antennas in silicon: Transmitter and local LO-path phase shifting," *IEEE J. Solid-State Circuits*, vol. 41, no. 8, pp. 2807–2819, Dec. 2006.
- [19] K. Scheir *et al.*, "A 52 GHz phased-array receiver front-end in 90 nm digital CMOS," in *IEEE Int. Solid-State Circuits Conf. (ISSCC) Dig. Tech. Papers*, 2008.
- [20] W. L. Chan *et al.*, "A 60 GHz-band  $2 \times 2$  phased-array transmitter in 65 nm CMOS," in *IEEE Int. Solid-State Circuits Conf. (ISSCC) Dig. Tech. Papers*, 2010, pp. 42–43.
- [21] P. Baltus *et al.*, "A 3.5 mW 2.5 GHz diversity receiver in silicon-on-anything," *IEEE J. Solid-State Circuits*, vol. 33, no. 12, pp. 2074–2079, Dec. 1998.
- [22] P. Baltus *et al.*, "Optimizing RF front ends for low power," *Proc. IEEE*, vol. 88, no. 10, pp. 1546–1559, Dec. 2000.
- [23] S. Kishimoto *et al.*, "A 60-GHz band CMOS phased array transmitter utilizing compact baseband phase shifters," in *IEEE Radio Frequency Integrated Circuits Symp. (RFIC)*, 2009.
- [24] K. Raczkowski *et al.*, "A wideband beamformer for a phased-array 60 GHz receiver in 40 nm digital CMOS," in *IEEE Int. Solid-State Circuits Conf. (ISSCC) Dig. Tech. Papers*, 2010, pp. 40–41.
- [25] A. Natarajan *et al.*, "A bidirectional RF-combining 60 GHz phased-array front-end," in *IEEE Int. Solid-State Circuits Conf. (ISSCC) Dig. Tech. Papers*, 2007, pp. 202–203.
- [26] K. Koh *et al.*, "An X- and Ku-band 8-element phased-array receiver in 0.18  $\mu\text{m}$  SiGe BiCMOS technology," *IEEE J. Solid-State Circuits*, vol. 43, no. 6, pp. 1360–1371, Jun. 2008.
- [27] K. Koh *et al.*, "A millimeter-wave (40–45 GHz) 16-element phased-array transmitter in 0.18  $\mu\text{m}$  SiGe BiCMOS technology," *IEEE J. Solid-State Circuits*, vol. 44, no. 5, pp. 1498–1509, May 2009.
- [28] A. Valdes-Garcia *et al.*, "A SiGe BiCMOS 16-element phased-array transmitter for 60 GHz communications," in *IEEE Int. Solid-State Circuits Conf. (ISSCC) Dig. Tech. Papers*, 2010, pp. 218–219.
- [29] Y. Yu *et al.*, "A 60 GHz digitally controlled RF-beamforming receiver front-end in 65 nm CMOS," in *IEEE Radio Frequency Integrated Circuits Symp. (RFIC)*, 2009.
- [30] S. Alalus *et al.*, "A 60 GHz phased array in CMOS," in *Proc. IEEE Custom Integrated Circuits Conf. (CICC)*, 2006, pp. 393–396.
- [31] Y. Yu *et al.*, "A 60 GHz digitally controlled phase shifter in CMOS," in *Proc. European Solid-State Circuits Conf. (ESSCIRC)*, 2008, pp. 250–253.
- [32] B. Min *et al.*, "Single-ended and differential Ka-band BiCMOS phased array front-ends," *IEEE J. Solid-State Circuits*, vol. 43, no. 10, pp. 2239–2250, Oct. 2008.
- [33] E. Cohen *et al.*, "A bidirectional TX/RX four element phased-array at 60 GHz with RF-IF conversion block in 90 nm CMOS process," in *IEEE Radio Frequency Integrated Circuits Symp. (RFIC)*, 2009.
- [34] M. Tsai *et al.*, "60 GHz passive and active RF-path phase shifters in silicon," in *IEEE Radio Frequency Integrated Circuits Symp. (RFIC)*, 2009.
- [35] K. Koh *et al.*, "0.13- $\mu\text{m}$  CMOS phase shifters for X-, Ku-, and K-band phased arrays," *IEEE J. Solid-State Circuits*, vol. 42, no. 11, pp. 2535–2546, Nov. 2007.
- [36] I. Sarkas *et al.*, "W-band 65-nm CMOS and SiGe BiCMOS transmitter and receiver with lumped I-Q phase shifters," in *IEEE Radio Frequency Integrated Circuits Symp. (RFIC)*, 2009.
- [37] J. Roderick *et al.*, "Silicon-based ultra-wideband beam-forming," *IEEE J. Solid-State Circuits*, vol. 41, no. 8, pp. 1726–1739, Aug. 2006.
- [38] T.-S. Chu *et al.*, "A true time-delay-based bandpass multi-beam array at mm-waves supporting instantaneously wide bandwidths," in *IEEE Int. Solid-State Circuits Conf. (ISSCC) Dig. Tech. Papers*, 2010, pp. 38–39.
- [39] J. A. G. Akkermans *et al.*, "Flip-chip integration of differential CMOS power amplifier and antenna in PCB technology for the 60-GHz frequency band," in *European Conf. Antennas and Propagation (EuCAP)*, 2009.
- [40] L. Tiemeijer *et al.*, "Predictive spiral inductor compact model for frequency and time domain," in *Int. Electron Devices Meeting (IEDM) Dig.*, 2003, pp. 36.4.1–36.4.4.
- [41] W. L. Chan *et al.*, "A 58–65 GHz neutralized CMOS power amplifier with PAE above 10% at 1-V supply," *IEEE J. Solid-State Circuits*, vol. 45, no. 3, pp. 554–564, Mar. 2010.
- [42] B. Martineau *et al.*, "A 53-to-68 GHz 18 dBm power amplifier with an 8-way combiner in standard 65 nm CMOS," in *IEEE Int. Solid-State Circuits Conf. (ISSCC) Dig. Tech. Papers*, 2010, pp. 428–429.



**Yikun Yu** received the B.Sc. degree in electrical engineering from Tsinghua University, Beijing, China, in 2002, and the M.Sc. degree (with honors) in electrical engineering from Delft University of Technology, Delft, The Netherlands, in 2005. In September 2005, he began working towards the Ph.D. degree at Eindhoven University of Technology, Eindhoven, The Netherlands.

During 2004–2005, he was with the Automotive Business Line, Philips Semiconductors, Nijmegen, The Netherlands. During 2007–2009, he was with NXP Semiconductors, Research, Eindhoven. In 2009, he joined IMEC, Eindhoven, as a research scientist. His research interests include analog, RF and millimeter-wave integrated circuit design.



**Peter G. M. Baltus** received the master's degree in electrical engineering from Eindhoven University of Technology, Eindhoven, The Netherlands, in 1985, and the Ph.D. degree from the same university in 2004.

He worked for 22 years at Philips and later NXP in various functions and locations. In 2007 he began his current job at the Eindhoven University of Technology as Professor in high-frequency electronics and Director of the Centre for Wireless Technology, Eindhoven. He holds 16 patents and coauthored

more than 30 papers.



**Anton de Graauw** received the Master of Science degree in electrical engineering from the Technical University of Delft, Delft, The Netherlands, in 1993.

He worked in several R&D positions for N.K.F. Telecom, Philips Components, Philips Semiconductors, and NXP in the areas of fiber-optic CATV systems, RF and mm-wave transceiver chips and Antenna modules. He currently works as a Senior Principal at the Integrated RF Solutions group of NXP Research in Eindhoven, The Netherlands.



**Edwin van der Heijden** graduated from the Eindhoven Polytechnic, The Netherlands, in 1994.

In 1996 he joined Philips Research Laboratories Eindhoven, where he has conducted research on high-frequency loadpull characterization of RF power transistors and on-wafer RF characterization of various active and passive devices in advanced IC processes. Since 1998 he has been involved in RF IC design on integrated transceivers. In 2006 he joined NXP Semiconductors.



**Cicero S. Vaucher** (M'98–SM'02) graduated in electrical engineering from the Federal University of Rio Grande do Sul, Porto Alegre, Brazil, in 1989. In 2001 he received the Ph.D. degree in the same field from the University of Twente, Enschede, The Netherlands.

From 1990 to 2006 he was with Philips Research Laboratories Eindhoven. In 2006 he joined the Research Department of NXP Semiconductors, where he is a Senior Principal in the Integrated RF Solutions group. His research activities and interests in-

clude implementations of low-power high-speed PLL frequency synthesizers, 60 GHz transceiver architectures and building blocks, modeling of mm-wave transceivers, and data/clock recovery and clock conversion circuits for optical transceivers. Currently, he is coordinating the European industrial and academic consortium "Qstream", towards realization of high-bit rate wireless data communication in the 60 GHz frequency band. He is the author of *Architectures for RF Frequency Synthesizers* (Kluwer, 2002) and is a coauthor of *Circuit Design for RF Transceivers* (Kluwer, 2001). He holds twelve U.S. patents, and has a number of applications pending.



**Arthur H. M. van Roermund** (SM'95) was born in Delft, The Netherlands in 1951. He received the M.Sc. degree in electrical engineering in 1975 from the Delft University of Technology and the Ph.D. degree in applied sciences from the K.U.Leuven, Belgium, in 1987.

From 1975 to 1992 he was with Philips Research Laboratories in Eindhoven. From 1992 to 1999 he was a full Professor at the Electrical Engineering Department of Delft University of Technology, where he was Chairman of the Electronics Research Group and a member of the management team of DIMES. From 1992 to 1999 he was Chairman of a two-year post-graduate school for "chartered designer." From 1992 to 1997 he was a consultant for Philips. In October 1999 he joined Eindhoven University of Technology as a full Professor, chairing the Mixed-signal Microelectronics Group. Since September 2002 he has also been Director of Research of the Department of Electrical Engineering. He is Chairman of the Board of ProRISC, a nationwide microelectronics platform; a member of the ICT research platform for The Netherlands (IPN); and a member of the supervisory board of the NRC Photonics research center. Since 2001, he has been one of the three organizers of the yearly workshop on Advanced Analog Circuit Design (AACD). In 2007 he was a member of an international assessment panel for the Department of Electronics and Information of Politecnico di Milano, and in 2009 for Electronics and Electrical Engineering for the merged Aalto University Finland. He has authored or coauthored more than 300 articles and 18 books.

In 2004 Dr. van Roermund received the Simon Stevin Meester Award for his scientific and technological achievements.